

N78-24049

RESULTS OF STATIC TESTS OF A 1/4-SCALE MODEL  
OF THE BOEING YC-14 POWERED-LIFT SYSTEM

James L. Hassell, Jr.  
NASA Langley Research Center

SUMMARY

One-quarter-scale static ground tests of the Boeing YC-14 powered-lift system were conducted for correlation with full-scale test results. The 1/4-scale model utilized a JT-15D turbofan engine to represent the CF6-50D engine employed on the YC-14 advanced medium STOL transport prototype aircraft. The tests included evaluation of static turning performance, static surface pressure and temperature distributions, fluctuating loads, and accelerations of portions of the wing, flaps, and fuselage. Results are presented for the landing flap configuration over an appropriate range of fan pressure ratio as affected by several variables including ground height and vortex generator modifications. Static turning angles of the order of 60° were obtained. The highest surface pressures and temperatures were concentrated over the upper surface of the flaps in the region immediately aft of the USB nozzle.

INTRODUCTION

Past NASA research on the upper-surface blowing (USB) concept has progressed from tests of small-scale powered models for evaluations of low-speed powered-lift performance, stability, and control (refs. 1 to 4) to tests of large-scale models powered by real turbofan engines for evaluations of the operational environment produced on the upper wing and flap surfaces by the concept (refs. 5 to 7). The data base provided by this research has provided a valuable foundation for further development of the USB concept. As a result of increased interest in USB and the performance potential indicated for such a system, the Boeing Company recently incorporated the USB concept in the YC-14 advanced medium STOL transport prototype. As indicated in figure 1, the YC-14 utilizes Coanda flaps in conjunction with USB nozzles to provide low-speed powered lift. It will be noted, however, that the airplane uses D-nozzles to provide efficient performance during low speed operations and at cruise. The D-nozzle, which has a semielliptical exit shape, represents a marked change in design from the high-aspect-ratio, rectangular nozzles previously studied by NASA in large-scale tests (refs. 5 and 6).

The development program for the YC-14 included full-scale static tests of the powered-lift system components shown in figure 2. These components included the CF6-50D engine, the USB nozzle, a stub wing, the USB flaps, and

an adjacent boiler plate section of the fuselage. Some of the results of these full-scale tests at Boeing's Tulalip test facility are presented in reference 8.

Boeing's full-scale static test of the YC-14 powered-lift system provided the impetus for reduced-scale tests at Langley using a small turbofan engine — the primary objective being to evaluate scaling relationships for the various technologies involved. Other objectives were to conduct exploratory powered-lift research with a cruise-configured nozzle and to evaluate a broader range of variables than practical at Tulalip because of the constraints in time and cost.

Evaluation of the scaling relationships will be accomplished later; the present paper is limited to a discussion of some of the 1/4-scale test results.

#### SYMBOLS

$A_{\text{primary}}$	geometric area of primary (hot flow) nozzle at mixing plane, $\text{cm}^2$ ( $\text{in}^2$ )
$A_{\text{secondary}}$	geometric area of secondary (fan flow) duct at mixing plane, $\text{cm}^2$ ( $\text{in}^2$ )
$F_A$	axial force, N (lbf)
$F_N$	normal force, N (lbf)
$h/b$	ratio of height of wing upper surface at USB nozzle exit to wing span
$\frac{\Delta p}{P_{\text{amb}}}$	surface static pressure ratio. $\frac{\text{Incremental local surface static pressure}}{\text{Ambient pressure}}$
$T_{\text{amb}}$	ambient temperature, $^{\circ}\text{C}$ ( $^{\circ}\text{F}$ )
$\frac{y}{b/2}$	nondimensional spanwise location, $\frac{\text{Spanwise distance from airplane center line}}{\text{Airplane wing semispan}}$
$\frac{z}{b/2}$	nondimensional normal location, $\frac{\text{Distance normal to local surface}}{\text{Airplane wing semispan}}$
$\delta_j$	jet turning angle, $\tan^{-1} \frac{F_N}{F_A}$ , deg

$\delta_{USB}$  tangency angle of the upper surface of the aft flap at the trailing edge measured with respect to wing chord plane, deg

$\eta$  thrust recovery efficiency,  $\frac{\sqrt{F_N^2 + F_A^2}}{\text{Thrust}}$

USB upper-surface blowing

#### DESCRIPTION OF MODEL

The Langley 1/4-scale model of the YC-14 powered-lift system and the static ground test apparatus is shown in figure 3. The model is powered by a JT-15D turbofan engine rated at 9786 N (2200 lbf) static thrust (as compared with 222.4 kN (50 000 lbf) thrust for the CF6-50D engine of the full-scale YC-14). The side door on the USB nozzle was tested only in the "door open" configuration corresponding to that used for powered-lift operation. This door has two functions: First, it provides the necessary nozzle area variation to obtain engine match conditions for both take-off and cruise, and second, in the open position for powered-lift operation, it helps spread the exhaust gas flow outboard over the Coanda flap span. Essentially all geometric details of the nozzle, wing, flaps, vortex generators, and fuselage are scaled from the YC-14. In this view the model is mounted at a scaled height above the ground corresponding to the full-scale test at Tulalip; the upper surface of the wing is 1.45 m (4.75 ft) above the surface, compared with 5.80 m (19 ft) for the full-scale configuration at Tulalip.

Figure 4 shows how the YC-14 USB nozzle was adapted to the JT-15D engine, which has a bypass ratio of 3.3 and a maximum fan pressure ratio of 1.4. (The CF6-50D engine has a bypass ratio of 4.4 and a maximum fan pressure ratio of 1.6.) The differences in engine characteristics forced a compromise in the 1/4-scale nozzle design; the primary and secondary areas at the mixing plane were adjusted to the values shown in figure 4 rather than being geometrically scaled. Basically, this design feature of the nozzle was compromised in order to match static pressures from the fan and core flows. All other geometric details of the YC-14 nozzle, such as the skewed plug primary, were retained in the 1/4-scale model. The purpose of the skewed plug primary is to direct the hot core flow to the top of the mixed flow nozzle and thereby minimize thermal problems on the wing and flaps.

Some of the characteristics of the JT-15D engine are compared with the CF6-50D engine in table 1. Aside from the very large difference in thrust, these two turbofan engines have somewhat similar characteristics. With both engines operating at a fan pressure ratio of 1.4, the fan and core velocities of the two engines correspond fairly well. This operating condition is about 66 percent maximum thrust for the CF6-50D engine. However, as a result of the

difference in bypass ratios, the exhaust flow in the 1/4-scale tests is composed of a larger proportion of core flow, resulting in the higher peak temperature at this operating condition. The temperature data of the 1/4-scale tests should therefore give conservative results as related to the YC-14 airplane.

A sketch of the 1/4-scale apparatus is presented in figure 5 to provide a description of the force measurement system. The entire model, including the bellmouth inlet, engine, nozzle, wing, flap, and fuselage, is supported on a floating frame which has strain gages forward and aft to measure normal force and a simple rod-rigged load cell to measure axial force. These measurements provide the magnitude and direction of the resultant force. The resultant force is the thrust recovered, and the direction of the resultant force is the jet turning angle  $\delta_j$ . In order to determine thrust, the forward engine mounts are pivoted in pillow blocks which are instrumented with strain gages to measure engine axial force. The aft engine mount is supported by an adjustable link with rod end bearings at the top and bottom. The USB nozzle is mounted to the engine case but does not touch the wing, the fuselage, or any other part of the floating frame structure. A rubber seal isolates the face of the engine from the bellmouth inlet. The output of the engine axial-force strain gage was calibrated against measured thrust with the wing, flaps, and fuselage removed, and the calibration obtained was used to determine measured thrust during subsequent testing with the wing, flaps, and fuselage in place. Thrust recovery efficiency  $\eta$  is then defined as the ratio of the thrust recovered to the measured thrust.

Sensor locations for other types of data are shown in figure 6. Static pressure ports and thermocouples were distributed uniformly over the wings and flaps and also over appropriate areas of the fuselage. Surface microphones and accelerometers were also positioned on the wing, flaps, and fuselage, and are described in reference 9.

In addition, pressure and temperature rakes were installed in both the engine fan ducts and in the primary nozzle, and the bellmouth inlet was instrumented to measure inlet mass flow. This engine instrumentation provided for determination of ideal thrust and, when related to the measured thrust, permitted evaluation of the nozzle velocity coefficient.

The fluctuating loads and acceleration data are currently being analyzed and will not be presented. The data discussed will therefore be limited to static turning performance, surface pressures and temperatures, and flow surveys as affected by several of the more important variables for the landing flap configuration which has a trailing-edge upper-surface angle of  $86.5^\circ$ .

The test variables included a range of flap deflections, thrust corresponding to far pressure ratios from 1.1 to 1.4, and heights above the ground corresponding to wheel contact height (5.80 m (19 ft) full scale), to an airborne height (9.14 m (30 ft) full scale), and to a free-air condition.

The effectiveness of vortex generators in aiding flow attachment is critical in this powered-lift concept where the designer has elected to avoid a high nozzle kickdown angle because of cruise performance considerations; the vortex generator configuration therefore was considered to be an important variable.

#### STATIC TURNING PERFORMANCE

Figure 7 shows the effect of vortex-generator deployment on static turning performance for the landing flap configuration. The data are presented in terms of the jet turning angle  $\delta_j$  and the thrust recovery efficiency  $\eta$  as functions of fan pressure ratio. The pressure ratio range of interest for the YC-14 operating in the landing approach is between 1.25 and 1.4. The results presented were obtained for an h/b value of 0.147, the height corresponding to the YC-14 with wheels on the ground. For this particular comparison the gap between the nozzle and the wing was unsealed. The results indicate deployment of the basic vortex generators provides about  $12^\circ$  improvement in jet turning angle with a decrease in thrust recovery efficiency of about 5 to 6 percent. Also, values of jet turning angle tend to decrease with increasing fan pressure ratio. These results demonstrate the effectiveness of retractable vortex generators in providing improved jet turning angle without resorting to a high nozzle kickdown angle which might unduly compromise cruise efficiency. At this point it should be acknowledged that the full-scale static tests at Tulalip produced  $5^\circ$  to  $6^\circ$  better static turning angle with vortex generators retracted and about  $8^\circ$  better turning angle with vortex generators deployed. These discrepancies are possibly related to the juncture between the USB nozzle and the wing upper surface. On the full-scale YC-14 there is no juncture; the floor of the nozzle is formed by the upper surface of the wing.

Figure 8 shows the effect of height above the ground on static turning performance. For this comparison the basic vortex generators are in the up position, and the clearance gap between the edge of the USB nozzle and the upper surface of the wing has been sealed to better represent the full-scale YC-14 nozzle arrangement. Results are presented for two ground heights: h/b values of 0.147, corresponding to a wheel-on-the-ground condition, and 0.232, corresponding to a condition wherein the YC-14 wing is at a height of 9.14 m (30 ft) above the runway. The results indicate only about a  $1^\circ$  improvement in jet turning angle and a few percent better thrust recovery efficiency at the higher height. The infinite ground height condition is yet to be tested.

In order to assure an adequate level of powered-lift performance in the landing approach condition, further improvement in static turning performance to values approaching  $60^\circ$  was needed, especially at the higher fan pressure ratios. As shown in figure 9, two modifications to the basic vortex generators were made in an attempt to improve the turning. The first modification simply

doubled the span of the outside pair of vortex generators so that more of the jet efflux would be affected and thereby reenergize the boundary layer at the knee of the flap better than with the basic vortex generators. The second modification retained the same increased span and also increased the incidence angle  $10^\circ$  on the outside pair. The rationale for this second modification was to intensify the vortices produced by the outside pair of vortex generators so as to further energize the boundary layer and thereby promote better flow attachment toward the trailing edge of the flaps.

Figure 10 presents the static turning performance obtained with the two vortex generator modifications as compared with the basic vortex generators. Both modifications improved the jet turning angle, especially at the important higher fan pressure ratios. The second modification provided a significant  $5^\circ$  or  $6^\circ$  improvement in jet turning angle at a cost of about 4 percent in thrust recovery efficiency.

#### SURFACE PRESSURE AND TEMPERATURE DISTRIBUTIONS

Figure 11 provides a basis for understanding the flow characteristics on the upper surface of the wing and flaps. Surface pressure ratio contours are shown plotted on the upper surface of the wing and flaps in the region aft of the USB nozzle. Negative values of pressure ratio indicate suction pressures and positive values indicate impact pressures. In addition to providing indications of good or poor flow attachment, this type of data is also valuable to the designer for the determination of steady-state static loads over portions of the wing and flaps. The case shown in figure 11 is for the landing flap configuration with the basic vortex generators deployed, for a value of  $h/b$  of 0.147 and for a fan pressure ratio of 1.36. Along the center line of the thrust axis, suction pressures occur almost to the trailing edge indicating excellent flow attachment, but regions of poor flow attachment are indicated both inboard adjacent to the fuselage and outboard toward the tip of the flap. A cross plot of the surface pressure ratios along the spanwise dashed line indicated on the aft flap in figure 11 provides a better indication of the degree of flow attachment.

Figure 12 presents the cross plot of aft flap pressures to show the effect of vortex generator modifications. Surface pressure ratio  $\Delta p/p_{amb}$  is plotted against the nondimensional span parameter  $\frac{y}{b/2}$  with negative values of pressure ratio upward. The locations of the center line and the side of the fuselage are indicated in the figure. The most dramatic improvement in flow attachment due to the vortex generator modifications occurs in the inboard area of the flaps adjacent to the fuselage. The jet turning angles for this pressure ratio of 1.4 (refer to fig. 10) are also indicated in figure 12 for the basic vortex generators and for each of the modifications. These pressure data therefore indicate that all the improvement in static turning angle resulted from the inboard vortex generator modification. The outboard modified vortex generator only penalized the thrust recovery efficiency.

Surface-temperature contours over the wing and flaps for the case with basic vortex generators deployed are presented in figure 13. The higher temperatures from the primary flow are concentrated near the center line, with peak values slightly above  $204^{\circ}\text{C}$  ( $400^{\circ}\text{F}$ ) on the flap system. Flap structures of suitable high-temperature-resistant alloys such as stainless steel should experience no problem in this environment. The surface temperatures in the region of wing structure present no problem, even for aluminum alloys. Although not presented in figure 13, temperatures on the side of the fuselage never exceeded  $60^{\circ}\text{C}$  ( $140^{\circ}\text{F}$ ).

#### FLOW SURVEYS

Various flow surveys were made to determine the extent of the jet efflux dispersion and to evaluate local flow conditions related to specific microphone locations. In order to obtain detailed velocity profiles of the flow adjacent to the wing and flap upper surfaces, a survey rake about 48.3 cm (19 in.) long having 25 total pressure probes and fewer static pressure and thermocouple probes was used. Discrete velocity measurements were obtained at each of the total pressure probe locations.

Figure 14 shows the results of some of the flow surveys for the case of vortex generators deployed at the highest fan pressure ratio. Velocity profiles near the center line are shown at the nozzle exit, at two locations on the flaps corresponding to microphone positions, and aft of the trailing edge of the flaps. The rake was positioned normal to the local surface for each location. The peak velocity at the nozzle exit was about 375 m/sec (1230 ft/sec) and decayed to about 251 m/sec (825 ft/sec) at the flap trailing edge. The profile begins to change appreciably on the forward flap and then shows considerable thickening over the aft flap element and at the trailing edge.

Figure 15 shows the results of rake surveys made over the span of the nozzle exit and the flap trailing edge with modified vortex generators deployed (modification 2). The data were also obtained at the highest value of fan pressure ratio of 1.4. In these plots the velocity data are presented in terms of constant velocity contours measured in the two planes indicated — at the nozzle exit and at the flap trailing edge. The plots are oriented to relate the spanwise extent of the USB nozzle to the flap span. The data show that the higher velocity flow from the primary nozzle is concentrated in the upper center of the USB nozzle, with some indication of spreading of the lower velocity fan flow beyond the projection of the nozzle due to the "door open" geometry. Much of the flow pattern at the nozzle exit is apparent at the flap trailing edge, and it should be noted that the higher velocity flow is still concentrated along a projection of the nozzle center line. The flow was thickened 3 to 4 times the nozzle depth but has spread very well across the flap span. Of particular interest is the further indication of good flow attachment at the flap trailing edge near the side of the fuselage which was brought about by the modified vortex generators.

#### CONCLUDING REMARKS

Preliminary results of static tests of the 1/4-scale Boeing YC-14 USB model indicate that the static turning performance of the landing flap configuration was improved appreciably by the use of the basic vortex generator design. Regions of poor flow attachment were noted near the trailing edge of the flap both inboard adjacent to the fuselage and outboard toward the tip. Improved flow attachment was obtained by tailoring the vortex generators which resulted in further improvement in static turning performance. Peak values of surface static pressures and temperatures were concentrated over the upper surface of the flaps along the center line of the thrust axis. These results together with results dealing with fluctuating loads, currently under analysis, will be correlated with full-scale YC-14 static data with an eventual objective of establishing appropriate scaling laws for the various technologies involved.

## REFERENCES

1. Phelps, Arthur E.; Letko, William; and Henderson, Robert L.: Low-Speed Wind-Tunnel Investigation of a Semispan STOL Jet Transport Wing-Body With an Upper-Surface Blown Jet Flap. NASA TN D-7183, 1973.
2. Phelps, Arthur E., III; and Smith, Charles C., Jr.: Wind-Tunnel Investigation of an Upper Surface Blown Jet-Flap Powered-Lift Configuration. NASA TN D-7399, 1973.
3. Sleeman, William C., Jr.; and Hohlweg, William C.: Low-Speed Wind-Tunnel Investigation of a Four-Engine Upper Surface Blown Model Having a Swept Wing and Rectangular and D-Shaped Exhaust Nozzles. NASA TN D-8061, 1975.
4. Phelps, Arthur E., III: Wind-Tunnel Investigation of a Twin-Engine Straight-Wing Upper-Surface Blown Jet-Flap Configuration. NASA TN D-7778, 1975.
5. Staff of the Langley Research Center: Wind-Tunnel Investigation of the Aerodynamic Performance, Steady and Vibratory Loads, Surface Temperatures and Acoustic Characteristics of a Large-Scale Twin-Engine Upper-Surface Blown Jet-Flap Configuration. NASA TM X-72794, 1975.
6. Shivers, James P.; and Smith, Charles C., Jr.: Static Tests of a Simulated Upper Surface Blown Jet-Flap Configuration Utilizing a Full-Size Turbofan Engine. NASA TN D-7816, 1975.
7. Carros, Robert J.; Boissevain, Alfred G.; and Aoyagi, Kiyoshi: Aerodynamic Characteristics of a Large-Scale Hybrid Upper Surface Blown Flap Model Having Four Engines. NASA TM X-62460, 1975.
8. Sussman, M. B.; Harkonen, D. L.; and Reed, J. B.: USB Environment Measurements Based on Full-Scale Static Engine Ground Tests. Powered-Lift Aerodynamics and Acoustics, NASA SP-406, 1976. (Paper no. 30 of this compilation.)
9. Schoenster, James A.; Willis, Conrad M.; Schroeder, James C.; and Mixson, John S.: Acoustic-Loads Research for Powered-Lift Configurations. Powered-Lift Aerodynamics and Acoustics, NASA SP-406, 1976. (Paper no. 26 of this compilation.)

Table 1.- Comparison of Engine Characteristics

	CF6-50D	JT-15D
Rated thrust, kN (lbf) . . . . .	222.4 (50 000)	9.79 (2200)
Bypass ratio . . . . .	4.4	3.3
Fan pressure ratio . . . . .	1.6	1.4
Fan velocity, m/sec (ft/sec) . . . . .	<sup>a</sup> 255 (836)	255 (836)
Core velocity, m/sec (ft/sec) . . . . .	<sup>a</sup> 347 (1140)	375 (1230)
Peak exhaust gas temperature, K (°R) . . . . .	<sup>a</sup> 700 (1260)	872 (1570)

<sup>a</sup>Values at 66 percent maximum thrust, corresponding to a fan pressure ratio of 1.4.



Figure 1.- Boeing YC-14 advanced medium STOL transport.

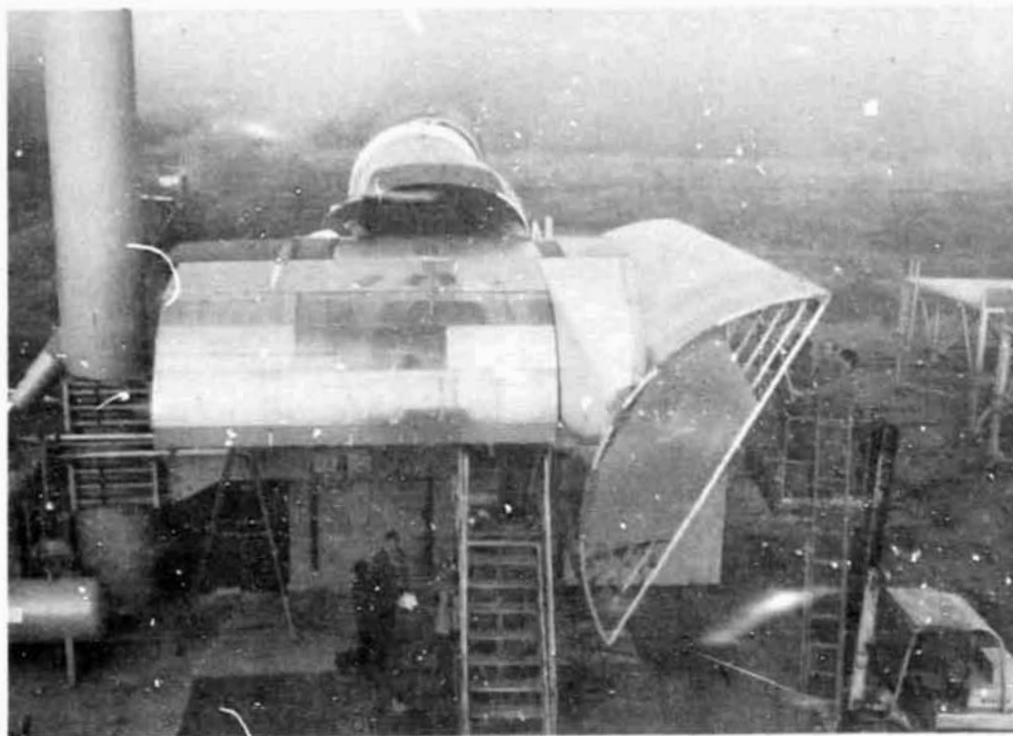


Figure 2.- Boeing's YC-14 Tulalip ground test.

ORIGINAL PAGE IS  
OF POOR QUALITY

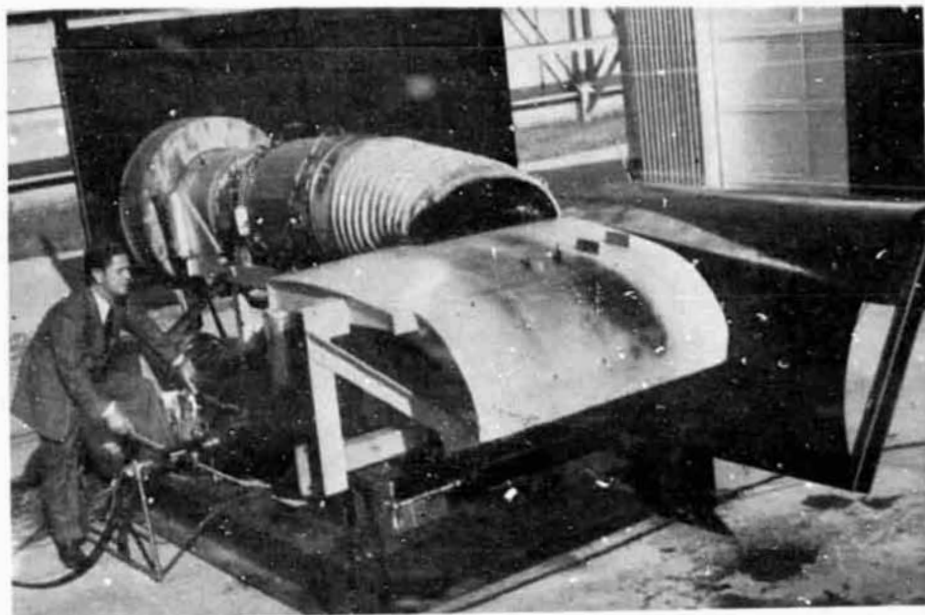


Figure 3.- 1/4-scale YC-14 ground test apparatus.

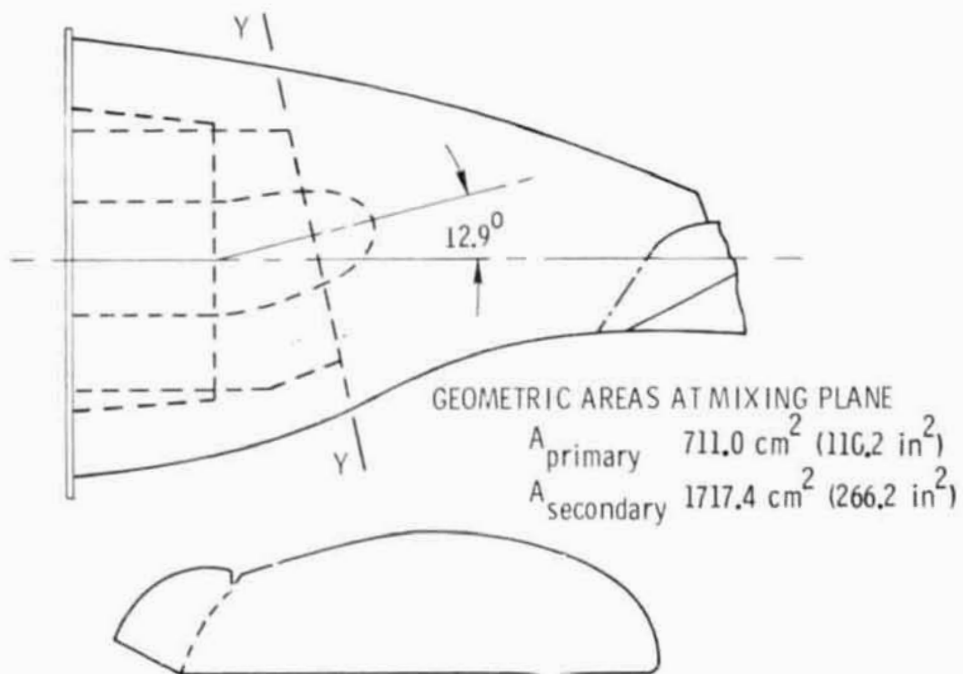


Figure 4.- YC-14 USB nozzle matched with JT-15D turbofan engine.  
Bypass ratio of 3.3; fan pressure ratio of 1.4.

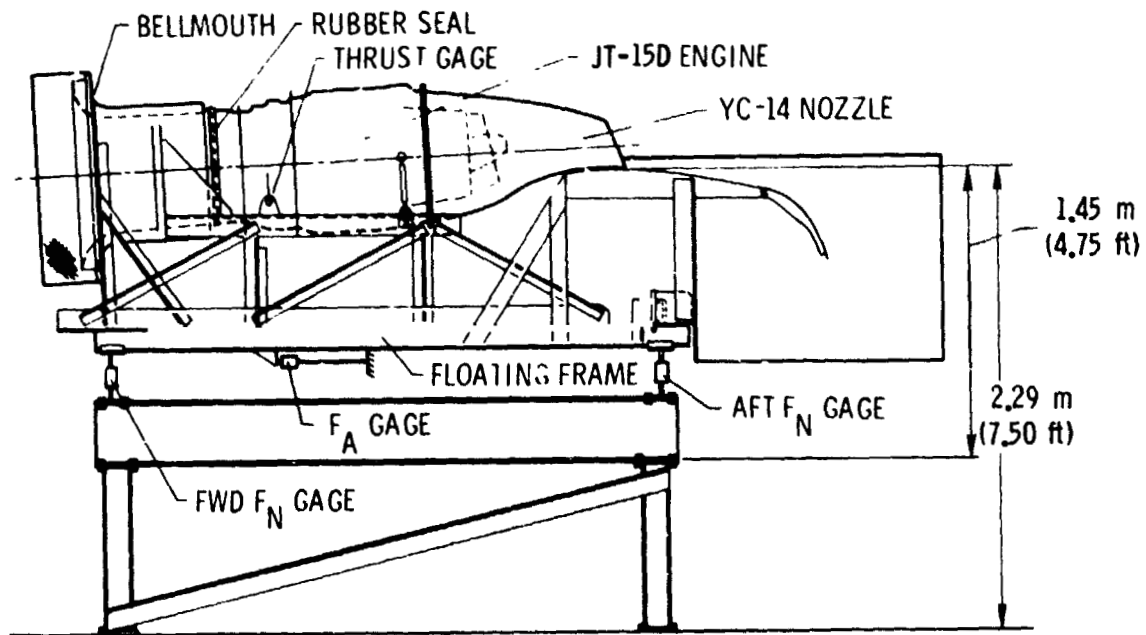
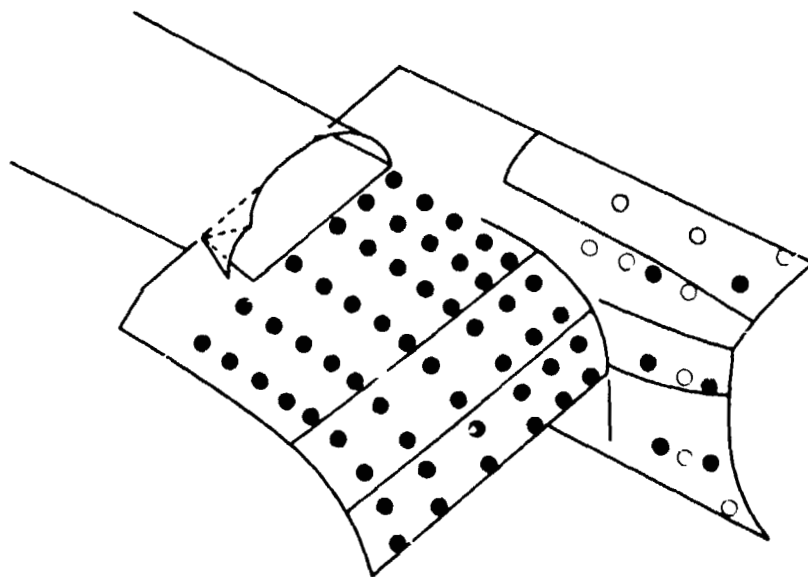


Figure 5.- Force measurement system for 1/4-scale ground tests.



- STATIC PRESSURE PORTS ONLY
- STATIC PRESSURE PORTS AND THERMOCOUPLES

Figure 6.- Sensor locations on wing, flaps, and fuselage.

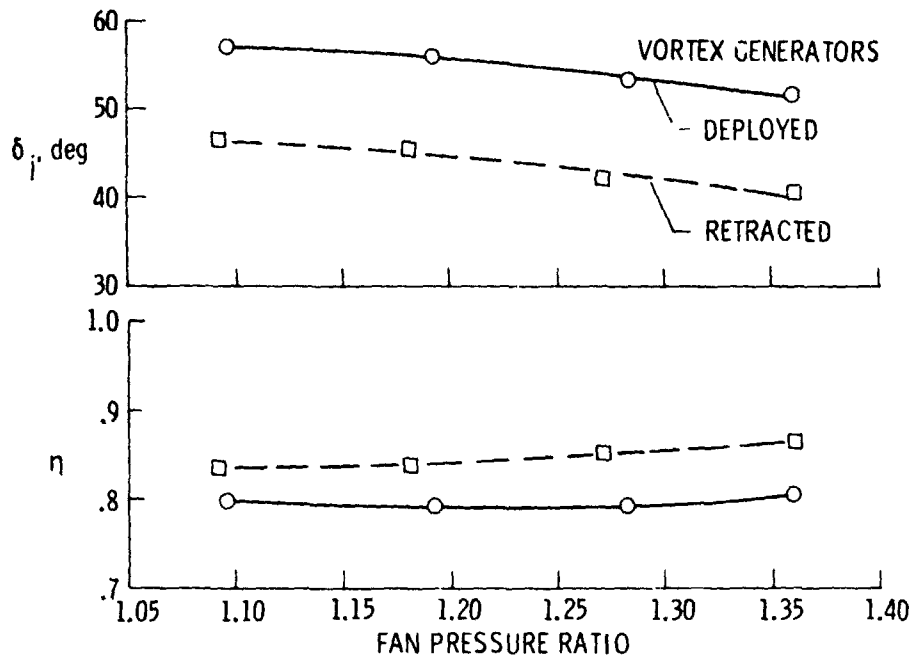


Figure 7.- Effect of basic vortex generators on static turning performance.  
 $h/b = 0.147$ ; nozzle-wing gap unsealed.

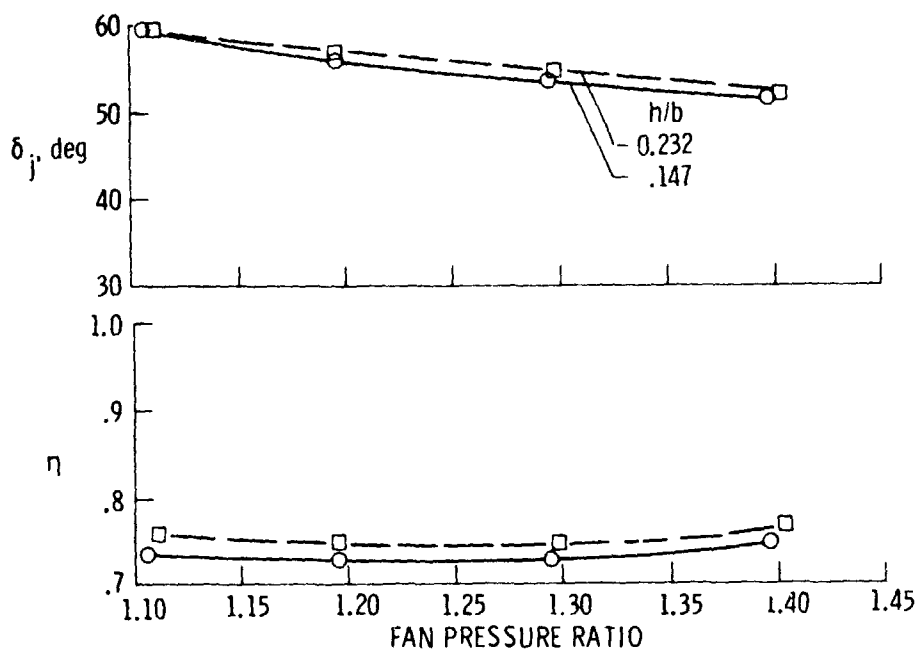


Figure 8.- Effect of height above ground on static turning performance.  
 Basic vortex generators up.

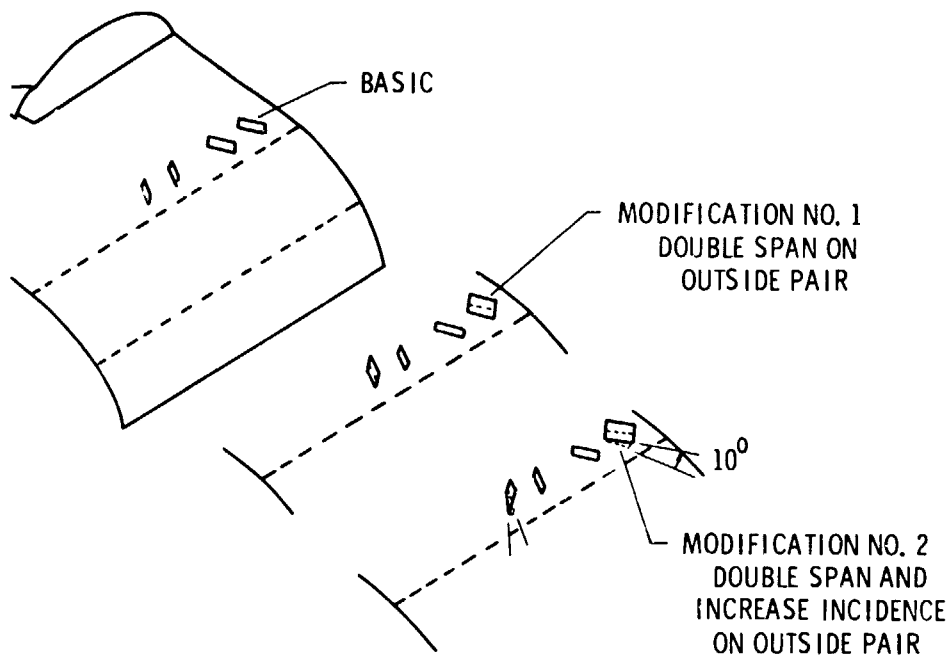


Figure 9.- Vortex generator modifications.

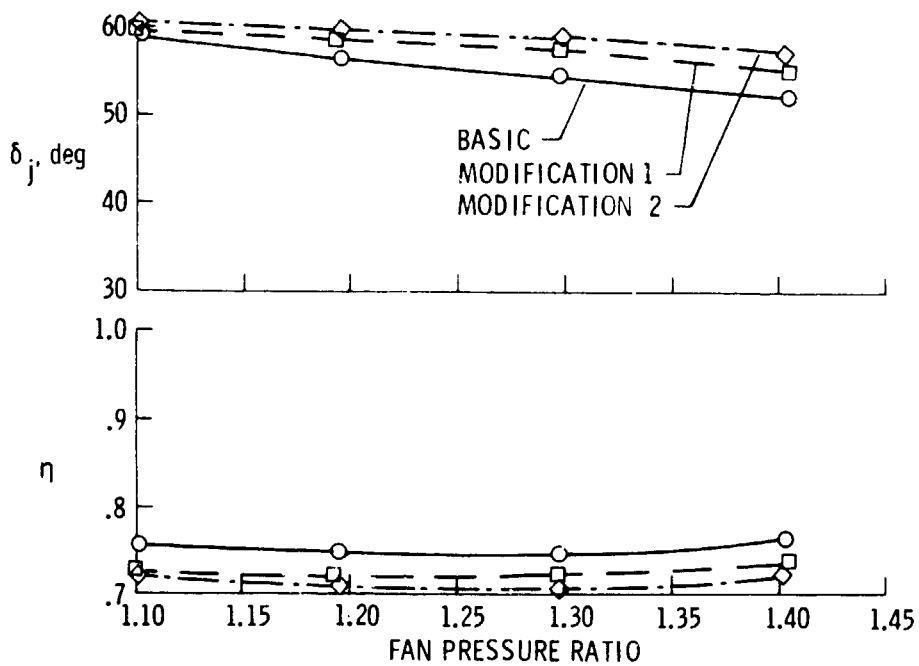


Figure 10.- Effect of vortex generator modifications on static turning performance.

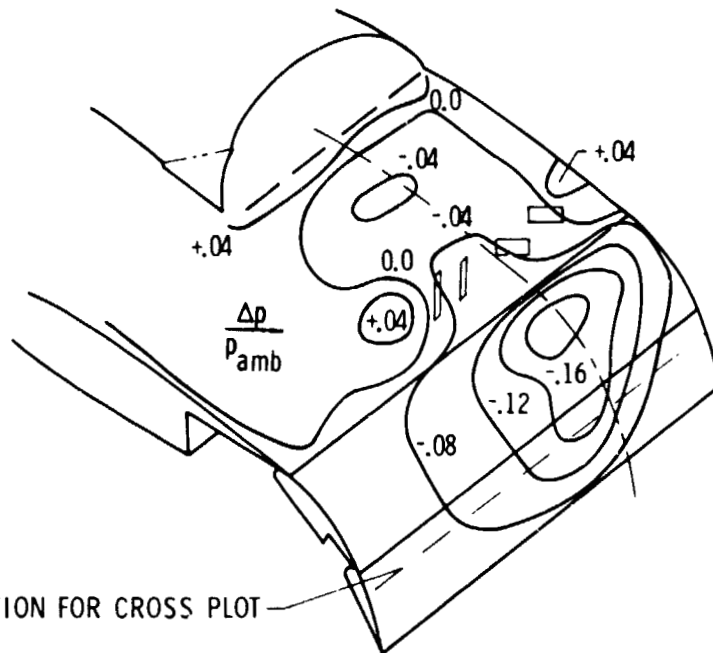


Figure 11.- Surface pressure ratio contours with basic vortex generators up.  $\delta_{USB} = 86.5^\circ$ ;  $h/b = 0.147$ ; fan pressure ratio of 1.36.

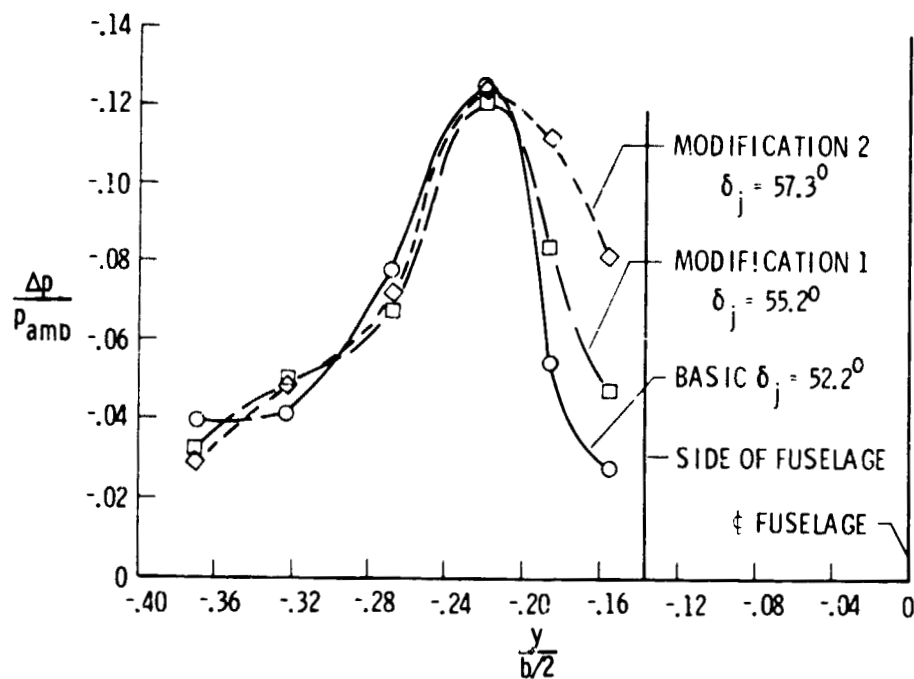


Figure 12.- Effect of vortex generator modifications.

$^{\circ}\text{F}$	$^{\circ}\text{C}$
100	38
200	93
250	121
300	149
350	177
400	204
420	216

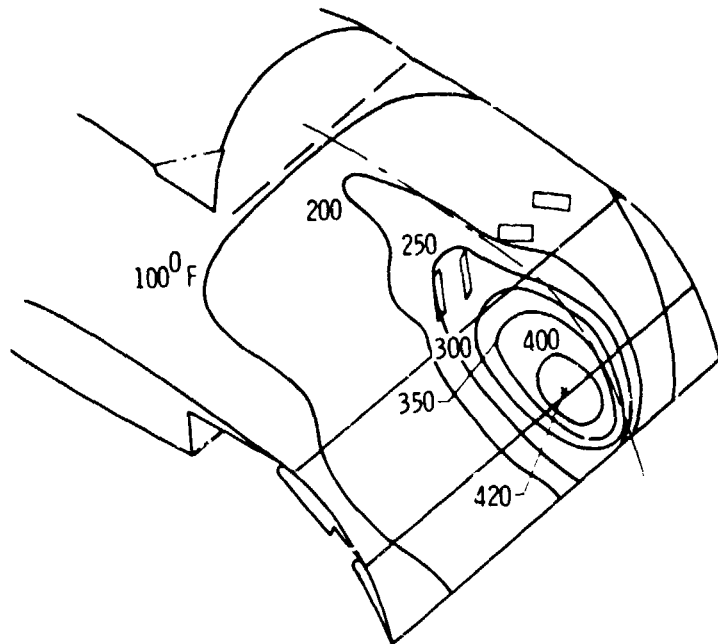


Figure 13.- Surface temperature contours with basic vortex generators up.  $\delta_{\text{USB}} = 86.5^{\circ}$ ;  $h/b = 0.147$ ;  $T_{\text{amb}} = 11^{\circ}\text{C}$  ( $52^{\circ}\text{F}$ ); fan pressure ratio of 1.36.

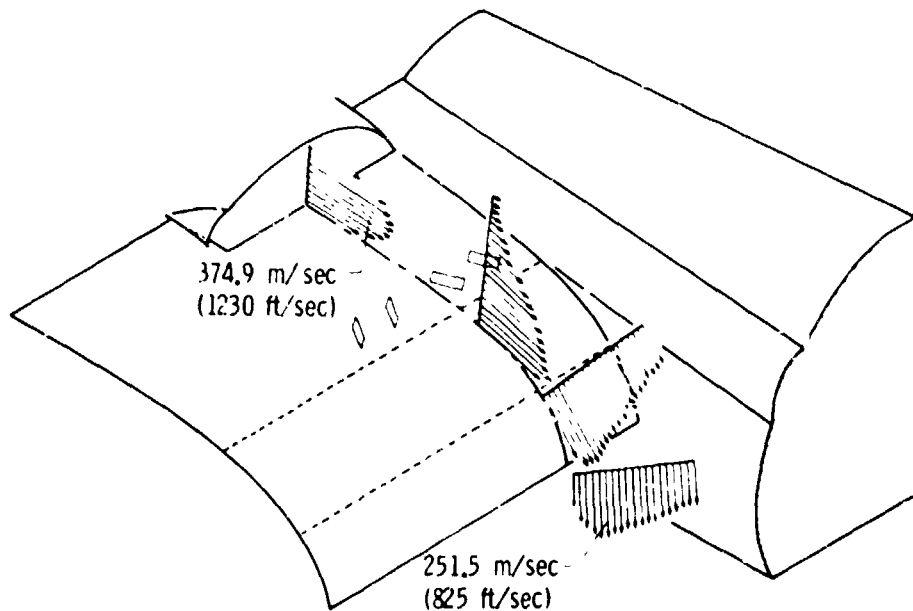


Figure 14.- Velocity profiles from nozzle exit to trailing edge.  $\delta_{\text{USB}} = 86.5^{\circ}$ ; basic vortex generators up.

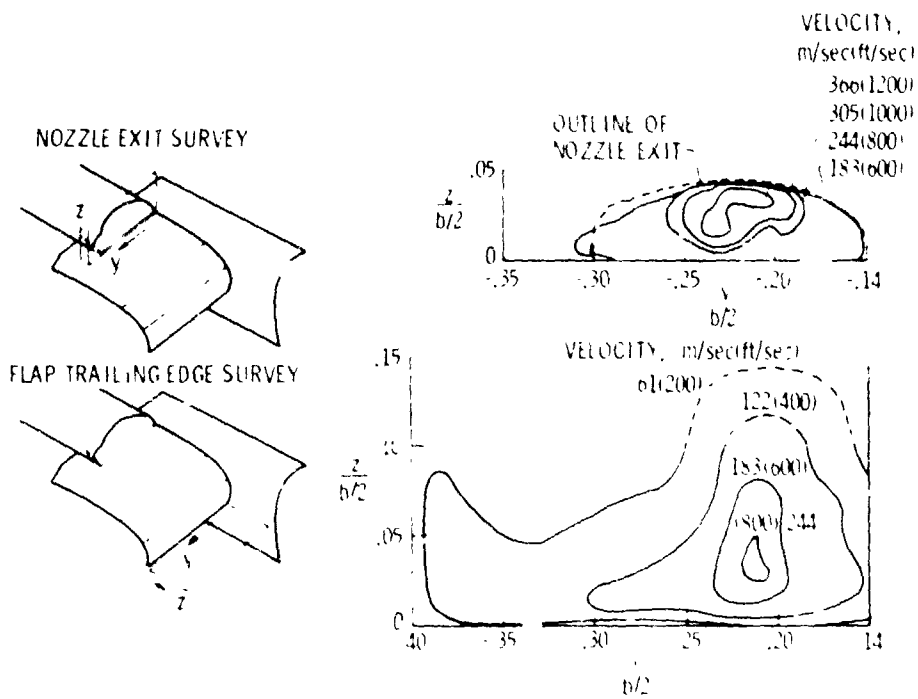


Figure 15.- Velocity contours at nozzle exit and flap trailing edge with modified vortex generators (modification 2). Fan pressure ratio of 1.4.

ORIGINAL PAGE IS  
OF POOR QUALITY